The Arginine 276 Anchor for NADP(H) Dictates Fluorescence Kinetic Transients in 3α-Hydroxysteroid Dehydrogenase, a Representative Aldo−Keto Reductase†

Kapila Ratnam, Haiching Ma, and Trevor M. Penning*

Department of Pharmacology, University of Pennsylvania School of Medicine, Philadelphia, Pennsylvania 19104-6084

Received December 2, 1998; Revised Manuscript Received March 29, 1999

ABSTRACT: Fluorescence stopped-flow studies were conducted with recombinant rat liver 3α-HSD, an aldo-keto reductase (AKR) that plays critical roles in steroid hormone inactivation, to characterize the binding of nicotinamide cofactor, the first step in the kinetic mechanism. Binding of NADP(H) involved two events: the fast formation of a loose complex (E·NADP(H)), followed by a conformational change in enzyme structure leading to a tightly bound complex (E*·NADP(H)), which was observed as a fluorescence kinetic transient. Binding of NAD(H) was not characterized by a similar kinetic transient, implying a difference in the mode of binding of the two cofactors. Unlike previously characterized AKRs, the rates associated with the formation and decay of E·NADP(H) and E*·NADP(H) were much faster than k_{cat} for the oxidoreduction of various substrates, indicating that binding and release of cofactor is not rate-limiting overall in 3α-HSD. Mutation of Arg 276, a highly conserved residue in AKRs that forms a salt bridge with the adenosine 2′-phosphate of NADP(H), resulted in large changes in K_m and K_d for NADP(H) that were not observed with NAD(H). The loss in free energy associated with the increase in K_d for NADP(H) is consistent with the elimination of an electrostatic link. Importantly, this mutation abolished the kinetic transient associated with NADPH binding. Thus, anchoring of the adenosine 2′-phosphate of NADPH by Arg 276 appears to be obligatory for the fluorescence kinetic transients to be observed. The removal of Trp 86, a residue involved in fluorescence energy transfer with NAD(P)H, also abolished the kinetic transient, but mutation of Trp 227, a residue on a mobile loop associated with cofactor binding, did not. It is concluded that in 3α-HSD, the time dependence of the change in Trp 86 fluorescence is due to cofactor anchoring, and thus, Trp 86 is a distal reporter of this event. Further, the loop movement that accompanies cofactor binding is spectrally silent.

Hydroxysteroid dehydrogenases (HSDs[1]) convert potent steroid hormones into their cognate inactive metabolites and, thus, regulate the occupancy and activation of steroid hormone receptors in steroid target tissues. HSDs belong to two protein superfamilies: short-chain dehydrogenases (SDR) (*1*) and aldo-keto reductases[2] (AKR) (*2*, *3*). Virtually all mammalian 3α-HSDs are members of the AKR superfamily. Hepatic 3α-HSDs inactivate circulating steroid hormones (*4*), while human prostate type 2 3α-HSD regulates the occupancy of the androgen receptor by converting 5α-dihydrotestosterone (a potent androgen) to 3α-androstanediol (a weak androgen) (*5*). Rat and human 3α-HSD isoforms have in excess of 69% sequence identity, and mechanistic studies on one are likely to be applicable to the rest.

Rat liver 3α-HSD, the first HSD to be identified as an AKR, displays an ordered bi-bi kinetic mechanism in which the nicotinamide cofactor binds first and leaves last (*6*). Reduction of a 3-ketosteroid substrate occurs by hydride transfer from the C4 position of the nicotinamide ring to the acceptor carbonyl at the C3 position of substrate, which is then protonated by a general acid. The reaction is stereospecific, with the 4-pro-*R* hydrogen being transferred from the A-face of cofactor to the β-face of steroid (*6*). The chemical mechanism, which has been recently elucidated, indicates that the enzyme operates by a "push−pull" mechanism involving three amino acids in the active site, Tyr 55, His 117, and Lys 84 (*7*). In the reduction direction, Tyr 55 acts as the general acid by donating a proton to the 3-ketosteroid substrate, a process facilitated by His 117. In the oxidation direction, Tyr 55 acts as the general base and abstracts a proton from the steroid alcohol, but in this case the reaction is facilitated by Lys 84.

The binding of the nicotinamide cofactor to AKRs is different from other oxidoreductases in that it is bound in an extended conformation (*8*−*10*). Examination of the macroscopic rate constants determined in the steady state for the kinetic mechanism of 3α-HSD suggests that the binding of cofactor is the slowest binding event, but it is

† This work was supported by NIH Grant DK47015 to T.M.P.

* To whom correspondence should be addressed: Department of Pharmacology, University of Pennsylvania School of Medicine, 3620 Hamilton Walk, Philadelphia, PA 19104-6084. Tel: (215) 898-9445. Fax: (215) 573-2236. E-mail: penning@pharm.med.upenn.edu.

[1] Abbreviations: HSD, hydroxysteroid dehydrogenase; 3α-HSD, 3α-hydroxysteroid dehydrogenase (EC 1.1.1.213, A-face specific and now designated as AKR1C9); AKR, aldo-keto reductase; SDR, short-chain dehydrogenase; IPTG, isopropyl β-D-thiogalactopyranoside; androsterone, 3α-hydroxy-5α-androstan-17-one; androstanedione, 5α-androstane-3,17-dione; 5α-dihydrotestosterone, 17β-hydroxy-5α-androstan-3-one; 3α-androstanediol, 5α-androstane-3α,17β-diol.

[2] The nomenclature for the aldo-keto reductase superfamily was recommended by the 8th International Symposium on Enzymology & Molecular Biology of Carbonyl Metabolism, Deadwood, SD, June 29−July 3, 1996 (*2*).

10.1021/bi982838t CCC: $18.00
Published on Web 05/27/1999

unknown whether this is rate-limiting overall (*6*). Previous studies on pig muscle aldose reductase, a related AKR, showed that the "off constant" for $NADP^+$ in the forward direction was 1 order of magnitude less than k_{cat} (*11*). Additionally, studies on human placental recombinant aldose reductase have shown that the movement of a nucleotide clamping loop (loop B) is the overall rate-limiting step in that enzyme (*12*). Binding of cofactor to both aldose reductases was kinetically observed by stopped-flow studies in which an E*·NADP(H) → E·NADP(H) isomerization event, prior to release of cofactor, was estimated to be the slowest step. A comparison of the crystal structure of apo3α-HSD with the 3α-HSD·$NADP^+$ complex indicates that there is a conformational change associated with binding of the nicotinamide cofactor that involves loop B adopting a more ordered state (*8*, *13*, *14*). However, the rate at which this conformational change occurs has not been determined, and hence, its influence on k_{cat} is unknown.

Fluorescence titrations with 3α-HSD indicate that the intrinsic protein fluorescence is quenched on binding NAD(P)(H), and that of the three tryptophans (Trp 86, Trp 227, and Trp 148) in the structure, Trp 86 is required for the energy-transfer band observed on binding reduced cofactor (*15*). In this work we extend our fluorescence studies to include stopped-flow measurements on the binding of all four natural nicotinamide cofactors to wild-type 3α-HSD and exploit the availability of the tryptophan mutants. We show that all events associated with cofactor binding and release are fast compared to k_{cat}, and the E·NADP(H) ⇄ D E*·NADP(H) event is not rate-limiting overall. The fluorescence kinetic transient observed upon binding NADP(H) is lost on mutating Arg 276, a residue conserved in AKRs that is implicated in anchoring the adenosine 2′-phosphate group of the dinucleotide. Further, we find that mutation of Trp 86 also abolishes the fluorescence kinetic transients, whereas mutation of Trp 227, on the mobile loop B, does not. Thus, Trp 86, a residue about 20 Å away from Arg 276, acts as a distal reporter of the anchoring event. By contrast, the movement of loop B that accompanies cofactor binding has no spectral signature. These studies may have implications for the binding of cofactor to other AKRs.

MATERIALS AND METHODS

Materials. Primers for PCR-based site-directed mutagenesis were purchased from GibcoBRL. The pET-16b expression vector was purchased from Novagen. *Escherichia coli* C41 (DE3) strain was kindly provided by Dr. J. E. Walker of the MRC Laboratory of Molecular Biology, Cambridge, U.K. Nicotinamide cofactors were obtained from Boehringer-Mannheim. Androsterone and androstanedione were purchased from Steraloids. All other reagents were ACS grade or better.

Mutagenesis, Expression, and Purification of Recombinant Wild-Type and Mutant 3α-HSDs. Generation and purification of the W86Y and W227Y mutants of 3α-HSD have been reported earlier (*15*). Construction of the expression plasmid pKK-3α-HSD and its use as a template to generate point mutations in 3α-HSD have been described previously (*16*). However, this vector does not always yield optimal expression of mutant 3α-HSDs. Hence, we generated the expression vector pET-3α-HSD by digesting pKK-3α-HSD with *Nco*I and *Bam*HI and ligating the fragment containing the cDNA for 3α-HSD into the inducible expression vector pET-16b. The R276M mutant was generated using PCR-based site-directed mutagenesis, by protocols described previously (*16*), using the pET-3α-HSD expression vector as template. The oligonucleotide primers used in the forward and reverse direction, respectively, were the following:

5′-dCCCCTGATCAGGAGTTTCAACGCGAAG-*ATG*ATCAAAGAGC-3′

5′-dGCTCTTTGAT*CAT*CTTCGCGTTGAAACT-CCTGATCAGGGG-3′

The italics denotes the mutated codon. The flanking forward and reverse primers used were 5′-dCCGGCTCGTATAATGTGTGGA-3′ and 5′-dCAGACCGCTTCTGCGTTCT-3′. Dideoxy sequencing ensured the fidelity of the mutant. The mutated expression vector was used to transform *E. coli* C41 (DE3) cells. The cells were grown in 4 L cultures of LB media, containing 100 μg/mL ampicillin, and upon reaching an A_{600} of 0.6, 1 mM IPTG was added to induce enzyme expression overnight. The protein was purified as described previously by sequential chromatography on a DE52 anion exchange and Sepharose Blue columns (*15*). Purity of the enzyme was verified by SDS−polyacrylamide gel electrophoresis, and protein concentration was determined by the method of Lowry (*17*). The homogeneous enzyme was stored in aliquots at −80 °C.

Steady-State Kinetics. Initial rates were measured using a Beckman DU-640C spectrophotometer by monitoring the formation or depletion of NADPH at 340 nm ($\epsilon = 6270\ M^{-1}\ cm^{-1}$). Assays were carried out in 1 mL systems in 100 mM potassium phosphate, pH 7.0, containing 4% acetonitrile, at 25 °C. Oxidation reactions were performed with 75 μM androsterone using varying concentrations of either $NADP^+$ (2−2300 μM) or NAD^+ (170−2300 μM). Reduction reactions were performed with varying concentrations of NADPH (0.6−12 μM) at 17 μM androstanedione and with varying concentrations of NADH (8−160 μM) at 34 μM androstanedione. In these instances steroid concentrations are saturating for wild type enzyme. Reactions were initiated by addition of enzyme. K_m and k_{cat} values were calculated using the ENZFITTER nonlinear regression analysis program (*18*) to fit data to a hyperbolic function. Control assays conducted with a range of potassium phosphate buffer concentrations (10−100 mM) showed no significant change in V_{max} in the presence and absence of 1 mM EDTA (T. M. Penning, unpublished data).

Rapid Reaction Kinetics. Rapid mixing experiments were performed using an Applied Photophysics SX.18MV stopped-flow reaction analyzer (dead time = 1.3 ms) at 25 °C. Enzyme and varying concentrations of nicotinamide cofactor solutions, in 10 mM potassium phosphate, pH 7.0, containing 1 mM EDTA, were introduced into the stopped-flow apparatus by means of separate syringes, and reactions were initiated by rapid mixing of the two solutions. Changes in the intensity of enzyme fluorescence emission were monitored at 336 or 450 nm following excitation at 290 nm. The kinetic transients obtained were analyzed and rate constants determined using Applied Photophysics SX.18MV v.4.32 software, based on a robust nonlinear regression (Marquardt)

algorithm or by the Pro-K global analysis and simulation software which uses the Marquardt−Levenberg nonlinear regression algorithm. All rate constants (k_{obs}) were determined from single-exponential fits to averages of 6−10 traces per cofactor concentration. Control experiments indicated that the presence of 4% acetonitrile did not result in significant changes in rate constants at different cofactor concentrations.

Data Analysis of Rapid Reaction Kinetics. Data obtained from stopped-flow experiments were replotted as k_{obs} versus [cofactor] (2−15 μM for NADPH and 2−25 μM for $NADP^+$). The data were fit to three models

$$E + NADP(H) \underset{k_2}{\overset{k_1}{\rightleftharpoons}} E{\cdot}NADP(H) \quad (1)$$

$$E + NADP(H) \underset{k_2}{\overset{k_1}{\rightleftharpoons}} E{\cdot}NADP(H) \xrightarrow{k_3} E^*{\cdot}NADP(H) \quad (2)$$

$$E + NADP(H) \underset{k_2}{\overset{k_1}{\rightleftharpoons}} E{\cdot}NADP(H) \underset{k_4}{\overset{k_3}{\rightleftharpoons}} E^*{\cdot}NADP(H) \quad (3)$$

Equation 1 predicts monophasic kinetic transients, and under conditions of [NADP(H)] ≫ [E], dependence of k_{obs} on NADP(H) concentration follows a pseudo-first-order rate equation (*19*, *20*). This model was discarded since saturation was achieved well below conditions for pseudo-first-order kinetics to apply and the predicted $K_d = k_2/k_1$ did not equal the K_d determined by fluorescence titrations (see below). Equations 2 and 3 predict biphasic kinetic transients but differ in that k_4 is not negligible in eq 3. Equation 3 was selected as the best model to explain our data, as k_4 was determined to be significant from stopped-flow experiments. Experimentally, the first event was fast, taking place within the dead time of the stopped-flow instrumentation, and a first-order rate constant for cofactor binding could not be determined. In this instance, the monophasic kinetic transients observed were a reflection of the subsequent isomerization event. The resultant plot of k_{obs} versus [cofactor] was hyperbolic, and the association of cofactor and enzyme was determined as a second-order rate constant (k_1) from the linear portion of this plot. The asymptote of the plot yielded a limiting rate constant (k_{lim}). A double-reciprocal plot of $1/k_{obs}$ versus 1/[NADP(H)] yielded $1/k_{lim}$, from the *y*-intercept. The two-step binding mechanism requires k_{lim} to be equal to either k_3 (eq 2) or ($k_3 + k_4$) (eq 3). It also predicts that, when k_4 has a finite value, at very low concentrations of cofactor, the expression for k_{obs} asymptotes to k_4 (*20*). Accordingly, the double-reciprocal plot plateaus at low cofactor concentrations, providing a limiting value of k_{obs} equal to k_4. Since k_4 was measurable and not negligible for 3α-HSD, eq 3 applies to our data. The dissociation constant (K_d for E·NADP(H), eq 3) and k_3 were determined from secondary analysis of experimental data. For example, a hyperbolic fit to the data in a plot of ($k_{obs} - k_4$) versus [cofactor] yielded k_3 and K_d. The rate of dissociation of cofactor from enzyme (k_2) was calculated from the equation $K_d = k_{off}/k_{on}$, where $k_{off} = k_2$ and $k_{on} = k_1$. In addition, we simulated individual transients, at the different cofactor concentrations, using the software KINSIM (*21*), as previously described by Grimshaw et al. (*12*), which yielded estimates of rate constants. The rate constants obtained by the different methods were in reasonable agreement (see Results).

Fluorescence Titrations with NAD(H), NADP(H). Binding of nicotinamide cofactors to the enzyme was measured by monitoring the quenching of intrinsic enzyme fluorescence upon incremental addition of cofactor. Emission spectra (300−450 nm) were recorded on a Perkin-Elmer 650−10S fluorescence spectrophotometer, following excitation at 290 nm. All titrations were performed in 1 mL volumes with 20 μg of enzyme in 10 mM potassium phosphate, pH 7.0. Care was taken to ensure that the volume of cofactor added was not more than 2% of the total volume, and appropriate corrections were made for changes in cofactor concentration. The data were plotted as a percent change in fluorescence at a fixed wavelength versus cofactor concentration. The dissociation constant (for E*·NADP(H), eq 3) is reported by fitting the data to a saturation absorption isotherm by the ENZFITTER nonlinear regression analysis program (*18*). Control experiments indicated that the presence of 4% acetonitrile did not result in significant changes in K_d.

RESULTS

Transient Kinetic Studies on Wild-Type 3α-HSD

Transient Kinetics of Cofactor Binding. Early studies characterizing the steady-state kinetic mechanism of rat liver 3α-HSD provided estimates of the rates of nicotinamide cofactor binding and release (*6*). Such measurements are reflections of overall events and cannot distinguish between the formation and decay of individual intermediates on the reaction pathway. To determine whether cofactor binding and release in 3α-HSD constituted one event or multiple events, we conducted transient-state kinetic studies by fluorescence stopped-flow methods, where [NADPH] and [$NADP^+$] were varied and fluorescence kinetic transients were observed at 336 nm (λ_{max} in the intrinsic fluorescence emission spectrum of 3α-HSD), following excitation at 290 nm (λ_{max} for the tryptophan fluorescence excitation spectrum) (*15*). Representative traces are shown in Figure 1, panels A and B, respectively. At all cofactor concentrations the kinetic transients exhibited monophasic behavior and fit to a single exponential, providing an estimate of k_{obs}. Kinetic transients were also detected at 450 nm (λ_{max} in the energy-transfer band observed on binding NADPH) (data not shown). The k_{obs} determined for the transients at 336 and 450 nm corresponded well, indicating that the binding of NADPH and formation of the energy-transfer band occurred simultaneously. Plots of k_{obs} versus [cofactor] showed that saturation was achieved at higher cofactor concentrations (Figure 1, panels A and B, inset). Hyperbolic fits to the plots for NADPH and $NADP^+$ yielded limiting rates (k_{lim}), and second-order rate constants for cofactor binding (k_1) were determined from the linear part of the plot (Table 1).

The kinetic behavior indicated that the binding of NADP(H) was in accordance with eq 3 (see Methods). Stopped-flow measurements were extended to include low cofactor concentrations, to enable determination of k_4 as the limiting rate obtained from a plot of $1/k_{obs}$ versus 1/[NADP(H)], as shown in Figure 2, panels A and B. For NADPH and $NADP^+$, k_4 was found to be 139 and 11 s^{-1}, respectively. Secondary plots of ($k_{obs} - k_4$) versus [NADP(H)] yielded estimates of k_3 (Figure 2). The same plot yielded a K_d of 5.5

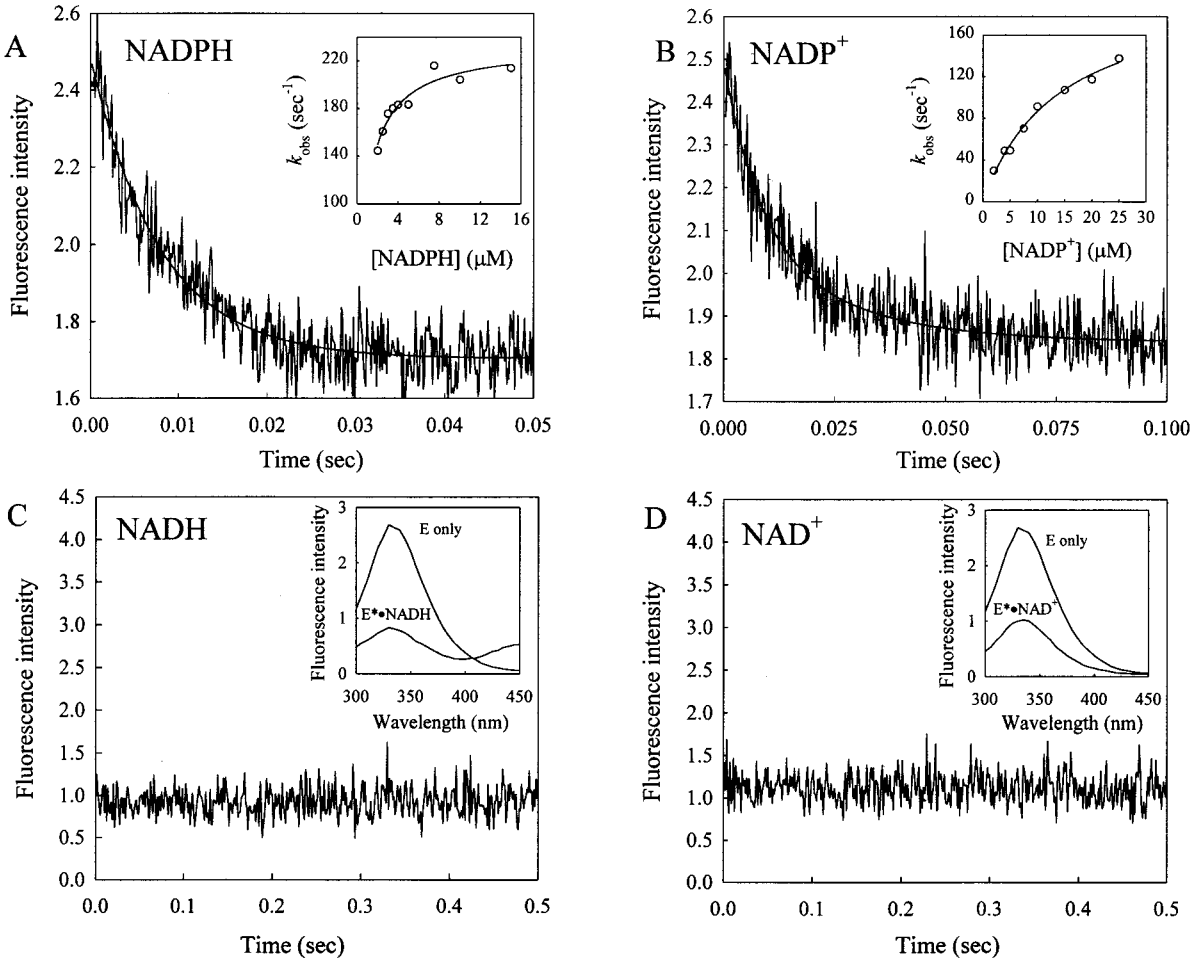

FIGURE 1: Representative fluorescence stopped-flow kinetic transients observed on binding nicotinamide cofactors with 3α-HSD. All reactions were carried out in 10 mM potassium phosphate buffer, pH 7.0, containing 1 mM EDTA, at 25 °C. Quenching of fluorescence emission with time was observed at 336 nm (λ_{ex} = 290 nm). (A) Reaction of 2 μM NADPH with 2 μM enzyme, fit to a single exponential; (inset) plot of k_{obs} versus [NADPH] with a hyperbolic fit to data. (B) Reaction of 10 μM $NADP^+$ with 2 μM enzyme, fit to a single exponential; (inset) plot of k_{obs} versus [$NADP^+$] with a hyperbolic fit to data. (C) Reaction of 350 μM NADH with 2 μM enzyme (identical traces were obtained from 7.5 to 350 μM NADH); (inset) fluorescence emission spectra of enzyme alone and enzyme in the presence of NADH. (D) Reaction of 800 μM NAD^+ with 2 μM enzyme (identical traces were obtained from 7.5 μM to 800 μM NAD^+); (inset) fluorescence emission spectra of enzyme alone and enzyme in the presence of NAD^+.

Table 1: Microscopic Rate Constants for the Formation and Decay of E·NADP(H) and E*·NADP(H)[a]

cofactor	k_{lim} (s^{-1})	k_1 ($M^{-1}\,s^{-1}$)	k_2 (s^{-1})	k_3 (s^{-1})	k_4 (s^{-1})	K_d (μM)
NADPH	233 ± 7	1.94 ± 0.03 × 10^7	107	107 ± 19	139 ± 6	6 ± 2
$NADP^+$	209 ± 14	7.5 ± 0.5 × 10^6	150	228 ± 22	11 ± 1	21 ± 4

[a] Determined in 10 mM potassium phosphate buffer, pH 7.0, containing 1 mM EDTA.

μM for NADPH and 20 μM for $NADP^+$. k_2 was calculated from the experimentally determined values of k_1 and K_d ($K_d = k_{off}/k_{on}$). The values for all the microscopic rate constants are listed in Table 1.

The K_d values determined for NADPH and $NADP^+$ from the stopped-flow experiments, listed in Table 1, are a reflection of the dissociation constants for the E·NADP(H) complex (eq 3). These values are 40- and 63-fold higher for NADPH and $NADP^+$, respectively, than those determined by fluorescence titrations, which are a measure of the K_d values for the E*·NADP(H) complex (Table 3). This difference, as measured by the two techniques, provides further evidence that the binding of cofactor to 3α-HSD involves two events as shown in eq 3.

3α-HSD has the ability to use NAD(H) as well as NADP(H) as cofactors in the oxidoreduction of a variety of substrates. Hence, we expected that the rapid reaction kinetics of cofactor binding observed with NADP(H) would be seen with NAD(H). Surprisingly, there were no kinetic transients associated with the binding of NAD(H) to 3α-HSD (Figure 1, panels C and D). The reaction was monitored over extended times and over a wide range of cofactor concentrations (7.5−350 μM for NADH and 7.5−800 μM for NAD^+) to ensure that any kinetic transient would be observed. The fact that NADH and NAD^+ bound to the enzyme within this time period was verified by recording the quench in the intrinsic enzyme fluorescence emission spectrum following cofactor binding (Figure 1, panels C and D, inset). These

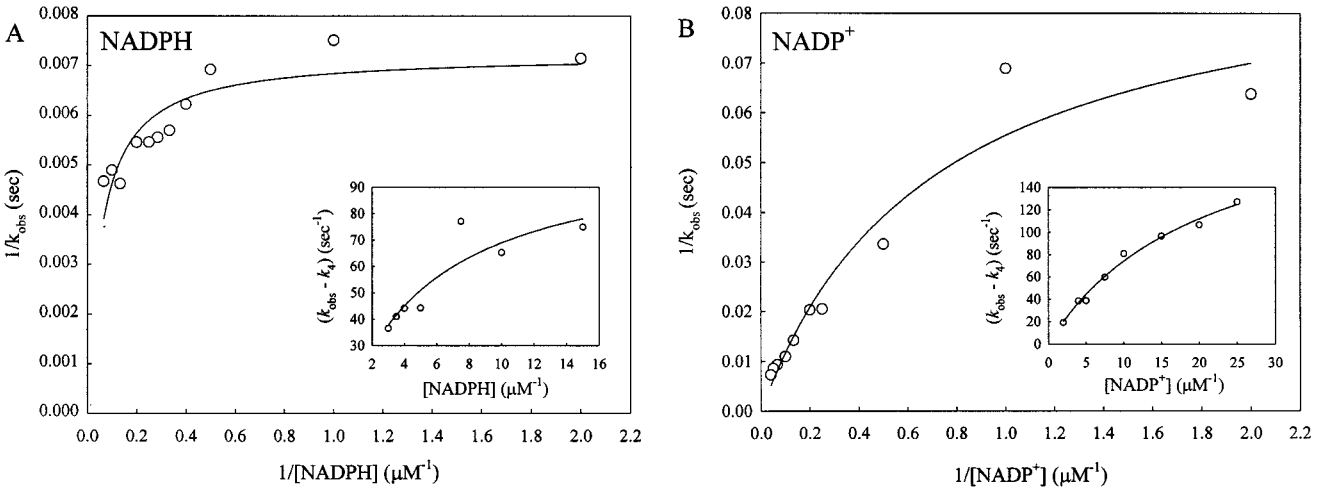

FIGURE 2: Double-reciprocal plots of k_{obs} versus [nicotinamide cofactor], extrapolating to finite values of k_4 at low cofactor concentrations. (A) Plot of $1/k_{obs}$ versus 1/[NADPH]; (inset) plot of ($k_{obs} - k_4$) versus [NADPH] with a hyperbolic fit to data. (B) Analogous plot with $NADP^+$.

data strongly suggest that 3α-HSD exhibits different modes of binding toward NAD(H) and NADP(H).

Comparison of k_4 and k_{cat}. In aldose reductase, a related AKR, the overall rate-limiting step is governed by the rate constant k_4 (defined in eq 3). This led to a comparison of k_4 and k_{cat} for 3α-HSD. The rate constant for release of NADPH from 3α-HSD is 139 s^{-1} and fast compared to a k_{cat} of 0.7 s^{-1} for androsterone oxidation (Table 2). For androstanedione reduction the k_{cat} is 0.3 s^{-1} compared to k_4 for $NADP^+$ release which is 11 s^{-1}. Also, simulation of experimental data using KINSIM (*21*) yielded reasonable results only when k_4 was set to be much larger than k_{cat}. Thus, dissociation of NADP(H) from 3α-HSD is not rate-limiting overall.

Mutagenesis and Cofactor Binding

Crystal structures of 3α-HSD (*8*, *14*) and studies with the related enzyme aldose reductase (*22*) implicate a conserved arginine (Arg 276 in 3α-HSD) in binding NADP(H) tightly, by forming an electrostatic link with the 2′-phosphate group, on the AMP moiety. Due to the absence of the 2′-phosphate group, this link cannot be formed with NADH. To test the hypothesis that Arg 276 is essential for the different modes of cofactor binding and therefore is obligatory for the fluorescence transients, we mutated this residue to a methionine. The effect of mutating tryptophan residues on the fluorescence transients was also measured.

Steady-State Kinetic Parameters of R276M for NADP(H) and NAD(H). The steady-state kinetic parameters of the R276M mutant were determined using $NAD(P)^+$ as cofactor for the oxidation of androsterone and NAD(P)H as cofactor for the reduction of androstanedione (Table 2). The greatest effect of this mutation was on the K_m value for all cofactors. With NAD(H) as cofactor, the K_m determined for R276M increased by about 6-fold. When NADP(H) was used as cofactor, however, the effect on K_m was much greater. The K_m values for $NADP^+$ and NADPH increased 106- and 32-fold, respectively. As a result, the catalytic efficiency of R276M decreased in all cases and mainly reflected the changes in K_m for cofactor. Overall, the R276M mutant had a greater effect on the steady-state kinetic parameters for NADP(H) than on NAD(H), consistent with the role of Arg 276 acting as an anchor for the adenosine 2′-phosphate.

Table 2: Comparison of Steady-State Kinetic Parameters for Wild-Type Enzyme and R276M[a]

cofactor		WT	R276M	ratio (R276M/WT)
NAD^+	k_{cat} (min^{-1})	76.4 ± 4.1	51.4 ± 17.7	0.67
	K_m (μM)	821 ± 124	5261 ± 2591	6.4
	k_{cat}/K_m (min^{-1} μM^{-1})	0.1	9.7×10^{-3}	0.1
NADH	k_{cat} (min^{-1})	25.9 ± 1.8	16.3 ± 1.1	0.62
	K_m (μM)	39.8 ± 8.3	229 ± 24	5.7
	k_{cat}/K_m (min^{-1} μM^{-1})	0.65	0.07	0.1
$NADP^+$	k_{cat} (min^{-1})	43.7 ± 0.1	49.7 ± 2.9	1.13
	K_m (μM)	5.2 ± 0.6	554 ± 80	106.6
	k_{cat}/K_m (min^{-1} μM^{-1})	8.4	0.09	0.01
NADPH	k_{cat} (min^{-1})	19.6 ± 1.4	28.6 ± 0.6	1.45
	K_m (μM)	1.9 ± 0.4	59.9 ± 3.9	31.5
	k_{cat}/K_m (min^{-1} μM^{-1})	10.3	0.5	0.05

[a] Determined in 100 mM potassium phosphate buffer, pH 7.0, containing 4% acetonitrile in the presence of saturating steroid concentrations for wild type enzyme. Steady-state kinetic parameters are not influenced by potassium phosphate buffer concentration (See Methods).

Table 3: Dissociation Constants of Cofactors for 3α-HSD and the R276M Mutant Determined by Fluorescence Titrations[a]

cofactor	K_d for WT (μM)	K_d for R276M (μM)	ratio (R276M/WT)
NADPH	0.14	18.7	133
$NADP^+$	0.32	44.5	139
NADH	114	8.4	0.07
NAD^+	263	37.9	0.14

[a] Determined in 10 mM potassium phosphate buffer, pH 7.0. Dissociation constants are not influenced by 4% acetonitrile (See Methods).

Comparison of the K_d Values of E·NADP(H) and E*·NAD(H) for Wild-Type Enzyme and the R276M Mutant.* The electrostatic interaction of the 2′-phosphate on the AMP moiety with Arg 276 is thought to be the primary cause for the lower K_d values exhibited by NADP(H) for wild-type 3α-HSD. We carried out fluorescence titration measurements using wild-type enzyme and the R276M mutant to determine the K_d values of all four cofactors (Table 3). The R276M mutant yielded the anticipated increase in K_d of NADPH and $NADP^+$, with the change being between 130- and 140-fold. Unexpectedly, the K_d of NADH and NAD^+ for R276M decreased by 14- and 7-fold, respectively, rather than

Table 4: Free-Energy Changes Associated with the Removal of Arg 276 or the Adenosine 2′-Phosphate on NADP(H)[a]

change introduced	enzyme/cofactor	$\Delta\Delta G_b$ (kcal/mol)
WT → R276M	NADPH	2.9
WT → R276M	$NADP^+$	2.9
WT → R276M	NADH	−1.5
WT → R276M	NAD^+	−1.2
NADPH → NADH	WT	3.9
NADPH → NADH	R276M	−0.4
$NADP^+ \rightarrow NAD^+$	WT	3.9
$NADP^+ \rightarrow NAD^+$	R276M	−0.1

[a] Energy changes were calculated using the following equation: $\Delta\Delta G_b = -RT \ln(K_d^{WT}/K_d^{R276M})$ as described (*23*, *24*).

remaining the same as wild-type. The changes in binding energy ($\Delta\Delta G_b$) on either mutating Arg 276 or on substituting NAD(H) for NADP(H) were calculated as described (*23*, *24*), using the following equation:

$$\Delta\Delta G_b = -RT \ln(K_d^{WT}/K_d^{R276M})$$

The results indicated that the increase in K_d of NADP(H) for R276M was associated with a free-energy change of about 3 kcal/mol and the energy change observed on replacing NADP(H) with NAD(H) for wild-type enzyme was 4 kcal/mol (Table 4). This energy change is consistent with the loss of an electrostatic link and is likely to be the single largest energetic contribution toward binding NADP(H). The decrease in K_d of NAD(H) for R276M yielded a free-energy change of about 1.5 kcal/mol, which is within the range of the energy associated with a hydrogen bond. Thus, it appears that in the R276M mutant a hydrogen bond is introduced, leading to the tighter binding of NAD(H).

Effect of Mutating Arg 276 on the Fluorescence Stopped-Flow Transients Observed on Binding NADPH. Our fluorescence stopped-flow experiments showed that there were kinetic transients associated with the binding of NADPH with wild-type enzyme, but none with the binding of NADH. It was concluded that the presence of the 2′-phosphate on the AMP moiety was necessary for the observation of the kinetic transients. To determine if the presence of Arg 276 was obligatory to observe the fluorescence kinetic transients, we monitored the binding of NADPH to R276M over a wide range of concentrations (2−120 μM) following rapid mixing in the stopped-flow apparatus. This wide range of concentrations was used to ensure that any kinetic transient would be detected. As a control, the quenching of the emission spectra of wild-type enzyme and the R276M mutant on binding NADPH were recorded, indicating that both enzymes bound cofactor (Figure 3A, B). Importantly, the fluorescence kinetic transients characteristic of NADPH binding to wild-type enzyme were absent in the R276M mutant (Figure 3C). This suggests that, when either Arg 276 or the 2′-phosphate on the AMP moiety is absent, anchoring of the cofactor via an electrostatic link no longer occurs. This interaction between the 2′-phosphate group and Arg 276 is essential if the fluorescence kinetic transient is to be observed. Thus, in 3α-HSD, it is the anchoring of NADP(H) which dictates the kinetic transients, and the movement of loop B appears to be spectrally silent.

Transient Kinetics of NADPH Binding to Tryptophan Mutants. Three tryptophan residues exist in 3α-HSD (Trp 86, Trp 227, and Trp 148), of which Trp 148 contributes

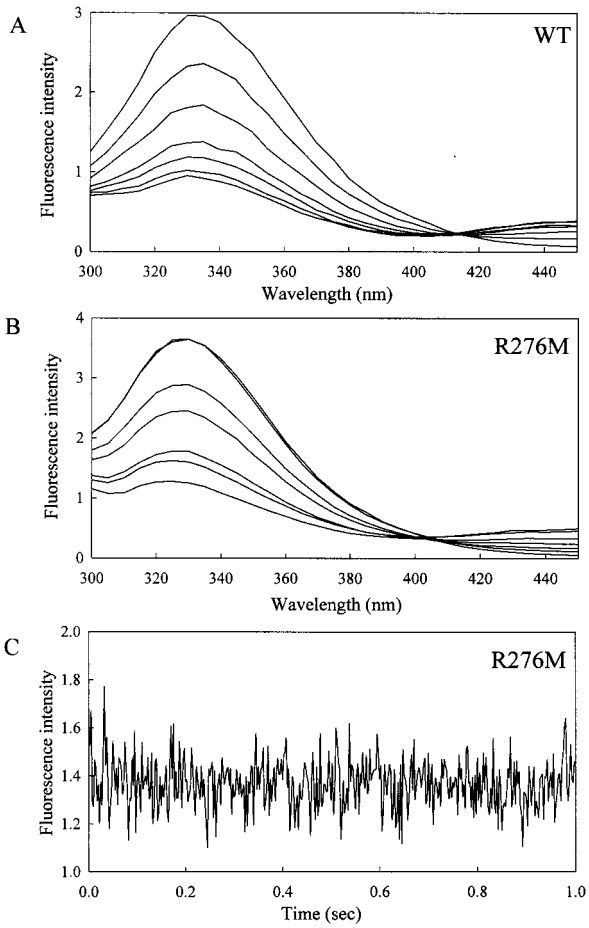

FIGURE 3: Comparison of binding of NADPH to wild-type 3α-HSD and R276M. All reactions were carried out in 10 mM potassium phosphate buffer, containing 1 mM EDTA, at 25 °C. Emission spectra and fluorescence kinetic transients were recorded at $\lambda_{ex} = 290$ nm. (A) Emission spectra of 2 μM wild-type 3α-HSD alone and on addition of 0.5, 1, 2, 3, 10, and 15 μM NADPH. (B) Emission spectra of 2 μM R276M alone and on addition of 4, 10, 20, 40, 60, and 80 μM NADPH. (C) Representative fluorescence transient observed at 336 nm during the reaction of 80 μM NADPH with 2 μM R276M (identical traces were obtained from 2 to 120 μM NADPH).

the most to intrinsic protein fluorescence but has little effect on cofactor binding or catalysis (*15*). We took advantage of existing tryptophan mutants, W86Y and W227Y, to investigate if these residues contribute to the fluorescence kinetic transients observed upon the binding of NADPH. Trp 86 and Trp 227 are in the vicinity of the cofactor binding pocket (*8*, *15*). Importantly, Trp 227 is found on the loop B that folds over cofactor following binding. By contrast, Trp 86 is found in an apolar cleft on the side opposite the mobile loop and lies further from the nicotinamide ring of the bound cofactor than Trp 227 (*8*). We conjectured that mutation of Trp 227 might abolish the fluorescence kinetic transient. However, the fluorescence kinetic transient was still observed when NADPH bound to the W227Y mutant, while it was completely lost on mutating Trp 86 (Figure 4). This indicates that the fluorescence kinetic transient associated with NADPH binding is not due to quenching of intrinsic protein fluorescence but is solely due to a specific interaction of the cofactor with Trp 86. Our studies indicate that Arg 276 is essential to anchor the adenosine 2′-phosphate of NADP(H), which in turn leads to the nicotinamide ring of the cofactor being locked into a specific orientation, permitting the

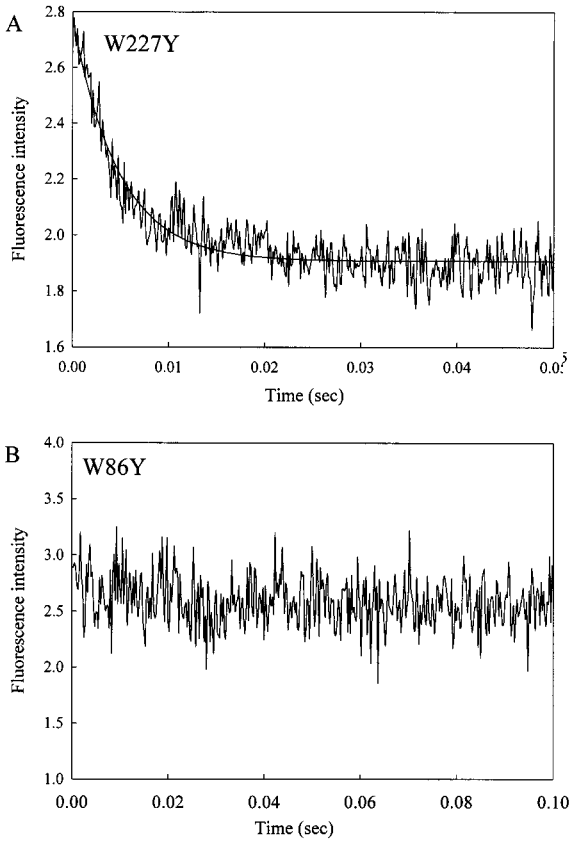

FIGURE 4: Representative fluorescence stopped-flow kinetic transients observed upon binding NADPH to the W227Y and W86Y mutants. All reactions were carried out in 10 mM potassium phosphate buffer, pH 7.0, containing 1 mM EDTA, at 25 °C. Quenching of fluorescence emission with time was observed at 336 nm (λ_{ex} = 290 nm). (A) Reaction of 10 μM NADPH with 2 μM W227Y mutant. (B) Reaction of 10 μM NADPH with 1.5 μM W86Y mutant (identical traces were obtained from 1.5 to 10 μM NADPH).

fluorescence kinetic transient associated with Trp 86 to be observed. Thus, Trp 86 acts as a distal reporter of the anchoring of NADP(H). In the absence of the anchoring event, the nicotinamide ring may adopt several orientations vis-à-vis Trp 86 and as a result the kinetic transient is absent.

DISCUSSION

In the study of AKR mechanisms, one of the primary concerns has been the identification of the rate-determining step. Steady-state kinetic studies with aldose reductase (*25*), an enzyme closely related to 3α-HSD, suggested that release of cofactor was the slowest step in the kinetic mechanism. Subsequently, detailed studies were performed to characterize the pre-steady-state kinetics of cofactor binding to pig muscle and human placental aldose reductase using fluorescence stopped-flow techniques (*11*, *12*). These studies showed that, rather than a simple binding mechanism, binding of cofactor involved two steps. Initially, a loose complex was formed between the cofactor and enzyme, followed by the formation of a tightly bound complex. Based on the crystal structure of aldose reductase (*9*), this tight complex was thought to arise due to the movement of loop B, which resulted in a fluorescence kinetic transient. By simulating the kinetics of cofactor binding to human aldose reductase, good fits to experimental data were obtained when k_4 was set equal to k_{cat}, and therefore, this step was judged to be rate-limiting overall in this enzyme. Our fluorescence stopped-flow studies show that, in 3α-HSD, fluorescence kinetic transients are due to the anchoring of NADP(H) by Arg 276 and this event is not the overall rate-limiting step in this enzyme.

Structural Interpretation of Kinetic Events. The observation that cofactor release from human aldose reductase is the rate-limiting step overall is supported by the crystal structure, where the cofactor was found to lie in a tunnel formed by loop B (*9*). The tunnel is maintained by electrostatic linkages between Asp 216 on the loop, Lys 21 on β1, and Lys 262 on α8 of the $(\alpha/\beta)_8$ barrel. The step defined by the rate constant k_4 in aldose reductase has been assigned to the breaking of these linkages and the opening of the tunnel prior to release of cofactor. A sequence alignment showed that 3α-HSD does not possess residues analogous to Lys 21 and Asp 216 in aldose reductase that could form a salt link and contribute to tunnel formation. Comparison of the crystal structures of 3α-HSD·$NADP^+$ (*8*) and 3α-HSD·$NADP^+$·testosterone complexes (*14*) with that of the apo-3α-HSD (*13*) indicated that there was indeed a conformational change on binding $NADP^+$, which involved loop B adopting a more ordered state while folding over the cofactor, but there was no obvious tunnel formed. Moreover, the pyrophosphate bridge of $NADP^+$ could be modeled in two conformations, indicating some flexibility in this region of the structure (*8*). Our fluorescence stopped-flow studies indicate that the event governed by the rate constant k_4 is the breaking of the link between NADP(H) and Arg 276. However, while it is likely that the movement of loop B occurs concomitantly with cofactor anchoring, there is no spectral signature associated with it, and hence, it cannot be observed by fluorescence stopped-flow techniques. Our observation that k_4 is faster than k_{cat} is in accord with the crystal structure of 3α-HSD and its complexes.

Factors Governing Association and Dissociation of NADP(H) from 3α-HSD. A plot of k_{obs} at different cofactor concentrations indicated that the binding of NADP(H) occurred in two steps, as defined by eq 3. Similar to aldose reductase, an initial loose complex was followed by the formation of a more tightly bound complex. However, our data suggest that there are significant differences between 3α-HSD and the mechanism proposed for aldose reductase. These are reflected primarily in the rate constants governing the different steps (Table 1). A comparison of these constants with the k_{cat} values determined for the oxidation or reduction of different substrates (*7*, *16*) indicates that all of the rate constants associated with cofactor binding or release are substantially higher than k_{cat}.

The K_d determined from the stopped-flow experiments is the dissociation constant for the initial complex, E·NADP(H) (Table 1). We were also able to determine the dissociation constants for the final complex (E*·NADP(H)) from fluorescence titration measurements (Table 3). A comparison of the two dissociation constants yielded about a 40- and 63-fold decrease in K_d, for NADPH and $NADP^+$, respectively, on formation of the tightly bound complex with 3α-HSD. These differences are much less than those observed for aldose reductase, where there was a 100- and 650-fold decrease in K_d for NADPH and $NADP^+$, respectively (*12*). These data together with evidence from the crystal structures

suggest that neither the anchoring event nor the associated movement of loop B, following binding of NADP(H), have the profound consequences for the kinetic mechanism of 3α-HSD that are exhibited in the case of aldose reductase. As k_{cat} reflects all of the steps in an ordered bi-bi reaction and is not governed by cofactor binding or release, this suggests that another step must be rate-limiting in 3α-HSD. Steady-state kinetic experiments show that formation of the ternary complex occurs faster than formation of the binary complex, implying that the chemical step must be rate-limiting overall (*6*). If this is so, then primary and solvent kinetic isotope effect experiments will identify the rate-limiting step.

Differences in the Modes of Binding of NADP(H) and NAD(H) with 3α-HSD: Arg 276 as the Adenosine 2′-Phosphate Anchor. 3α-HSD displays dual pyridine nucleotide specificity, with the K_m values being 57-fold higher for NADH than NADPH and 160-fold higher for NAD^+ than $NADP^+$ (Table 2). The enzyme also exhibits vastly different K_d values for the E*·cofactor complexes, as determined by fluorescence titrations, with the NADH/NADPH and NAD^+/$NADP^+$ ratios being 814 and 821, respectively (Table 3). This prompted us to determine the microscopic rate constants associated with NAD(H) binding, using fluorescence stopped-flow methods. However, no fluorescence kinetic transients associated with the isomerization of E·NAD(H) to E*·NAD(H) were observed, suggesting that the mode of binding of NADP(H) was different from that of NAD(H). The difference between the two forms of the oxidized and reduced cofactors is the presence of the 2′-phosphate on the AMP moiety, and it appears that this group is essential for the fluorescence kinetic transients to be observed. Crystal structures of the binary and ternary complexes suggest that the 2′-phosphate group forms a hydrogen bond and a salt bridge with Ser 271 and Arg 276, respectively (*8*, *14*). These interactions probably account for the lower K_d observed for the binding of NADP(H). The electrostatic link between Arg 276 on the enzyme and the 2′-phosphate group most likely imposes a specific orientation on NADP(H) which is reported concurrently by Trp 86 as a fluorescence kinetic transient. Anchoring of NADP(H) by Arg 276 is the second event described in eq 3, since the mutation of this residue eliminated the low K_d associated with the E*·NADP(H) complex. By contrast, NAD(H) cannot be anchored by this mechanism, presumably allowing the nicotinamide ring to adopt several orientations which is reflected in a high K_d, and the precise interaction with Trp 86 is disrupted. In the absence of the crystal structure of a binary complex with NAD(H), we can only speculate on its mode of binding to 3α-HSD. However, given that the binding of this cofactor may permit the ligand to adopt multiple orientations, an electron density map and, therefore, a crystal structure may be difficult to obtain for this complex.

Steady-state kinetic parameters determined with an R276M mutant indicated that removal of Arg 276 had a profound effect on the K_m and K_d for NADP(H) with much smaller effects on the parameters for NAD(H) (Table 2), as might be expected by the removal of the anchor. The change in free energy of 3 kcal/mol, associated with the removal of Arg 276 for NADP(H), is equivalent to that required for the formation of a salt bridge and is similar to the energy change observed with an analogous mutation in pig muscle aldose reductase (*22*). The difference in K_d between NADP(H) and NAD(H) with wild-type enzyme, however, gives rise to a change in free energy of 4 kcal/mol. This additional energy of 1 kcal/mol is most likely due to the remaining hydrogen bonding interaction between the adenosine 2′-phosphate on NADP(H) and Ser 271.

Our stopped-flow experiments with wild-type enzyme showed that the presence of the 2′-phosphate group on the AMP moiety of cofactor was necessary to orient the nicotinamide ring toward Trp 86 such that the kinetic transients could be observed. When stopped-flow experiments were conducted with the R276M mutant, no kinetic transients were observed with NADPH. Thus, despite the distance of about 20 Å from the C4 position of the nicotinamide ring, Arg 276 dictates the orientation of the nicotinamide ring and its interactions with Trp 86. These observations verify the essential nature of Arg 276 in forming an electrostatic link with the 2′-phosphate group on the AMP moiety. This residue is highly conserved in AKRs, and it is likely that its presence is responsible for the fluorescence kinetic transients observed in aldose reductase (*11*, *12*). If this is the case, then the fluorescence kinetic transient observed with aldose reductase is due to cofactor anchoring rather than movement of loop B, as is currently presumed.

Nature of the Fluorescence Transient: Trp 86 as a Reporter for the Kinetics of Cofactor Binding. 3α-HSD contains three tryptophans (Trp 86, Trp 227, and Trp 148) which contribute to intrinsic protein fluorescence to varying extents. Previous site-directed mutagenesis studies showed that Trp 148 was the largest contributor to protein fluorescence but had the least effect on cofactor binding and catalysis. All three tryptophans are quenched to some degree by cofactor. However, Trp 86 is solely responsible for the energy-transfer band associated with NAD(P)H binding (*15*). On the basis of their position in the crystal structure, we conjectured that Trp 227 might be responsible for the kinetic transient since it is on loop B, while Trp 86 is buried in an apolar cleft (*8*). Stopped-flow experiments with the W227Y and W86Y mutants showed that the kinetic transient was observed with the W227Y mutant but was absent in the case of the W86Y mutant. Since the fluorescence kinetic transient is due to Trp 86 alone, the signals responsible for the intrinsic protein fluorescence and the kinetic transient are clearly different. Importantly, the kinetic transient is observed only when a cofactor anchor forms and represents the finite time required to form an electrostatic linkage with the 2′-phosphate group of AMP. In the case of both NADH and wild-type enzyme, and NADPH and the R276M mutant, the transient is not observed as the anchor cannot form. However, in either case the energy-transfer band is still observed, although much larger concentrations of cofactor are now required to achieve this effect. In the absence of anchoring, the cofactor forms a loose complex and likely adopts several orientations versus Trp 86 and only one results in the energy-transfer band. Tryptophans analogous to Trp 86 and Trp 227 are found in other members of the AKR superfamily including aldose reductase (*26*). Although aldose reductase possesses two additional tryptophans which are within the vicinity of the nicotinamide ring, it seems probable that Trp 79, which is analogous to Trp 86 in 3α-HSD, is responsible for the fluorescence kinetic transient in aldose reductase.

Overall, the data presented here provide a lucid model of the kinetics of NADP(H) binding. The fast formation of the

E·NADP(H) complex occurs within the dead-time of the stopped-flow instrument. The slow event resulting in the formation of E*·NADP(H) is governed by anchoring with Arg 276 and accompanied by concurrent changes in the fluorescence properties of the reporter group Trp 86.

Implications for the AKR Superfamily. Among members of the AKR superfamily, the most well-characterized enzymes in terms of structure−function and their catalytic mechanisms are mammalian 3α-HSD, aldose reductase, and aldehyde reductase, and it is only natural to compare and contrast the behavior of these enzymes. They exhibit similar overall kinetic mechanisms and perform the same chemistry on a variety of substrates using similar catalytic machinery. All three enzymes possess conserved residues that perform similar functions, such as Arg 276 acting as the anchor for NADP(H). However, subtle changes in amino acid sequences between these enzymes also result in significant differences in substrate specificity and kinetic behavior. In aldose reductase, the isomerization event leading to the "unlocking" of cofactor from the binding pocket has been identified as the sole determinant of the rate-limiting step. Studies with aldehyde reductase, on the other hand, suggest that catalysis is limited predominantly by the chemical step with a partial contribution from the isomerization step (*27*). Our current study indicates that in 3α-HSD none of the steps involving cofactor binding or release are rate-limiting overall. A recently determined structure of the binary complex of 2,5-diketo-D-gluconic acid reductase A and NADPH, a prokaryotic member of the AKR superfamily, suggests that there is no extensive conformational change in loop B on binding cofactor and that this event will be governed by a simple reversible equilibrium (*28*). Thus, in spite of similarities in the overall structure and the reactions catalyzed by the various members of the AKR superfamily, a entire spectrum of cofactor binding behavior can be expected from these enzymes.

ACKNOWLEDGMENT

We thank Dr. Barry Cooperman for the use of the stopped-flow reaction analyzer and Dr. J. M. Vanderkooi for the use of the fluorescence spectrophotometers in their respective laboratories. We are grateful to Dr. J. M. Jez for many insightful discussions.

REFERENCES

1. Jornvall, H., Persson, M., Krook, M., Atrian, S., Gonzalez-Duarte, R., Jeffery, J., and Ghosh, D. (1995) *Biochemistry 34*, 6003−6013.
2. Jez, J. M., Flynn, T. G., and Penning, T. M. (1997) *Biochem. Pharmacol. 54*, 639−647.
3. Jez, J. M., Bennett, M. J., Schlegel, B. P., Lewis, M., and Penning, T. M. (1997) *Biochem. J. 326*, 625−636.
4. Tomkins, G. M. (1956) *J. Biol. Chem. 218*, 437−447.
5. Lin, H.-K., Jez, J. M., Schlegel, B. P., Peehl, D. M., Pachter, J. A., and Penning, T. M. (1997) *Mol. Endocrinol. 11*, 1971−1984.
6. Askonas, L. J., Ricigliano, J. W., and Penning, T. M. (1991) *Biochem. J. 278*, 835−841.
7. Schlegel, B. P., Jez, J. M., and Penning, T. M. (1998) *Biochemistry 37*, 3538−3548.
8. Bennett, M. J., Schlegel, B. P., Jez, J. M., Penning, T. M., and Lewis, M. (1996) *Biochemistry 35*, 10702−10711.
9. Wilson, D. K., Bohren, K. M., Gabbay, K. H., and Quiocho, F. A. (1992) *Science 257*, 81−84.
10. Wilson, D. K., Nakano, T., Petrash, J. M., and Quiocho, F. A. (1995) *Biochemistry 34*, 14323−14330.
11. Kubiseski, T. J., Hyndman, D. J., Morjana, N. A., and Flynn, T. G. (1992) *J. Biol. Chem. 267*, 6510−6517.
12. Grimshaw, C. E., Bohren, K. M., Lai, C.-J., and Gabbay, K. H. (1995) *Biochemistry 34*, 14356−14365.
13. Hoog, S. S., Pawlowski, J. E., Alzari, P. M., Penning, T. M., and Lewis, M. (1994) *Proc. Natl. Acad. Sci. U.S.A. 91*, 2517−2521.
14. Bennett, M. J., Albert, R. H., Jez, J. M., Ma, H., Penning, T. M., and Lewis, M. (1997) *Structure 5*, 799−812.
15. Jez, J. M., Schlegel, B. P., and Penning, T. M. (1996) *J. Biol. Chem. 271*, 30190−30198.
16. Pawlowski, J. E., and Penning, T. M. (1994) *J. Biol. Chem. 269*, 13502−13510.
17. Lowry, O. H., Rosenbrough, J. J., Farr, A. J., and Randall, R. J. (1951) *J. Biol. Chem. 193*, 265−275.
18. Leatherbarrow, R. J. (1987) *ENZFITTER: A Nonlinear Regression Data Analysis Program for the IBM PC (and True Compatibles)*, BioSoft, Cambridge, U.K.
19. Fierke, C. A., and Hammes, G. G. (1995) *Methods Enzymol. 249*, 3−37.
20. Strickland, S., Palmer, G., and Massey, V. (1975) *J. Biol. Chem. 250*, 4048−4052.
21. Barshop, B. A., Wrenn, R. F., and Frieden, C. (1983) *Anal. Biochem. 130*, 134−145.
22. Kubiseski, T. J., and Flynn, T. G. (1995) *J. Biol. Chem. 270*, 16911−16917.
23. Sem, D. S., and Kasper, C. B. (1993) *Biochemistry 32*, 11548−11558.
24. Fersht, A. (1985) *Enzyme Structure and Mechanism*, W. H. Freeman & Co., New York.
25. Grimshaw, C. E., Shahbaz, M., and Putney, C. G. (1990) *Biochemistry 29*, 9947−9955.
26. Bohren, K. M., Bullock, B., Wermuth, B., and Gabbay, K. H. (1989) *J. Biol. Chem. 264*, 9547−9551.
27. Barski, O. A., Gabbay, K. H., Grimshaw, C. E., and Bohren, K. M. (1995) *Biochemistry 34*, 11264−11275.
28. Khurana, S., Powers, D. B., Anderson, S., and Blaber, M. (1998) *Proc. Natl. Acad. Sci. U.S.A. 95*, 6768−6773.

BI982838T